Methods and Applications in Fluorescence

PAPER

An approach to estimate spatial distribution of analyte within cells using spectrally-resolved fluorescence microscopy*

RECEIVED
25 August 2016

REVISED
29 October 2016

ACCEPTED FOR PUBLICATION
15 November 2016

PUBLISHED
18 January 2017

Dharmendar Kumar Sharma[1], Mir Irfanullah[1], Santanu Kumar Basu[2], Sheri Madhu[1], Suman De[1], Sameer Jadhav[2], Mangalampalli Ravikanth[1] and Arindam Chowdhury[1]

[1] Department of Chemistry, Indian Institute of Technology Bombay, Powai, Mumbai 400 076, India
[2] Department of Chemical Engineering, Indian Institute of Technology Bombay, Powai, Mumbai 400 076, India
* Dedicated to Professor Kankan Bhattacharyya.

E-mail: arindam@chem.iitb.ac.in

Keywords: intracellular sensing, spectral imaging, colorimetric sensors, multiparameter analysis, single-cell analysis, microspectroscopy, fluorescence imaging

Supplementary material for this article is available online

Abstract

While fluorescence microscopy has become an essential tool amongst chemists and biologists for the detection of various analyte within cellular environments, non-uniform spatial distribution of sensors within cells often restricts extraction of reliable information on relative abundance of analytes in different subcellular regions. As an alternative to existing sensing methodologies such as ratiometric or FRET imaging, where relative proportion of analyte with respect to the sensor can be obtained within cells, we propose a methodology using spectrally-resolved fluorescence microscopy, via which both the relative abundance of sensor as well as their relative proportion with respect to the analyte can be simultaneously extracted for local subcellular regions. This method is exemplified using a BODIPY sensor, capable of detecting mercury ions within cellular environments, characterized by spectral blue-shift and concurrent enhancement of emission intensity. Spectral emission envelopes collected from sub-microscopic regions allowed us to compare the shift in transition energies as well as integrated emission intensities within various intracellular regions. Construction of a 2D scatter plot using spectral shifts and emission intensities, which depend on the relative amount of analyte with respect to sensor and the approximate local amounts of the probe, respectively, enabled qualitative extraction of relative abundance of analyte in various local regions within a single cell as well as amongst different cells. Although the comparisons remain semi-quantitative, this approach involving analysis of multiple spectral parameters opens up an alternative way to extract spatial distribution of analyte in heterogeneous systems. The proposed method would be especially relevant for fluorescent probes that undergo relatively nominal shift in transition energies compared to their emission bandwidths, which often restricts their usage for quantitative ratiometric imaging in cellular media due to strong cross-talk between energetically separated detection channels.

1. Introduction

Over the last few decades, fluorogenic sensing has emerged to be one of the most useful tools for analyte detection both in solution and cellular medium [1–8]. Chromophores chemically modified with appropriate functional groups (receptors) for sensing of various chemicals, biochemicals and ions use the alteration of photophysical characteristics (such as quantum yield, transition energy and excited state lifetime) of the reporter units upon detection/binding to analyte [5–8]. A vast majority of fluorescent sensors are based on changes in the quantum-efficiency of the reporter units (fluorescence quenching or turn-on), which work very efficiently in homogeneous medium (solution) to detect micromolar to nanomolar concentration of analyte [9, 10]. With the ease in availability of fluorescence microscopes, sensing measurements are routinely being performed to confirm the existence of analyte within cellular environments (under physiological conditions), typically by monitoring the *average* change in emission intensity (or relative change in average emission intensity) of the sensor over a large number of cells [11–13]. On the contrary however, in spite of recent developments in high-resolution optical microscopy, it is rather challenging

© 2017 IOP Publishing Ltd

to extract information on the relative amounts of analyte in various intracellular regions simply using emission intensity of sensory probes [3, 4, 14, 15]. This is primarily because, unlike a homogeneous solution, intracellular medium is quite heterogeneous (in terms of polarity, viscosity, etc) and most often, sensory probe molecules are not distributed uniformly throughout a cell [3, 14–16]. This poses a serious problem to estimate analyte distribution within individual cells, as intensity changes due to analyte detection cannot be effectively discriminated from those arising due to sensor concentration in various local regions of a cell [17, 18].

To avoid the difficulties of fluorescence intensity measurements to sense analyte in cellular environments, alternate methods such as fluorescence lifetime imaging microscopy (FLIM) and spectral-shift based imaging have become increasingly popular over the last two decades [4–7, 19–22]. FLIM has the advantage of being sensor concentration independent (for moderately low concentrations) [21] and has been used to sense biologically relevant parameters such as intracellular viscosity [23] and temperature [24] as well as to visualize cellular uptake/release of ions [19, 20]. However, the average radiative lifetimes, which typically increase with analyte binding, are also known to be extremely sensitive to the varying cellular (local) environments (such as polarity, rigidity etc) and often observed multi-exponential decay can be difficult to interpret [15, 19, 22]. Apart from FLIM, sensors which undergo significant spectral shift upon analyte binding (such as colorimetric or energy/electron transfer based sensors) have also been used for the detection of analyte within cells [7, 17, 25–27]. It should be mentioned that both lifetime and ratiometric imaging measurements on cells provide spatially resolved information on the relative proportion of analyte bound to sensors (with respect to free sensors), rather than the actual distribution of analyte within intracellular regions. For instance, identical intensity ratio (at two wavelengths), or average radiative lifetime obtained for two different microscopic regions within a cell does not necessarily imply that amount of *analyte* is identical because that would also depend on the local concentration of the sensor at those two locations[3]. Indeed, using ratiometric or lifetime imaging assays, intracellular spatial distribution of analyte can be obtained semi-quantitatively if the *same* cell is investigated in the absence and presence of the analyte, i.e. by monitoring systematic changes in the measured signal from the sensor at specific subcellular locations as a function of time or analyte concentration.

In this context, it is important to note that colorimetric or Förster resonance energy transfer (FRET) based ratiometric imaging for cellular sensing typically use fluorescence intensity images acquired through energetically separated emission filters [4, 25, 28]. While ratiometric image analyses is quite reliable when emission spectra of the sensor is not very wide and the spectral shifts are prominent, there can be serious crosstalk between the two detection channels when change of transition energy due to analyte detection is nominal (10–30 nm) with respect to the line-width of the fluorophores (typically ~30–70 nm). In this context, spectrally-resolved fluorescence microscopy (SRFM) can be used as a potential alternate for existing methods, as extraction of entire emission spectral profiles from various sub-microscopic locations within cellular media allow to discern subtle spectral changes along with information on the total intensity of emitted light. It is a surprise that despite of such advantages, sensing measurements using SRFM have not yet being used to its full potential, and there are only a few literature reports where spatially-resolved spectroscopy is being used for sensing local pH [29], viscosity [30] and for the detection of analyte [17, 18] in cellular environments.

In a prior report, we had used spatially resolved fluorescence spectroscopy to detect spectral shifts of a Boron-dipyrromethene (BODIPY) based colorimetric sensor for the detection of mercury ions inside cellular media [17]. However, due to non-uniform sensor distribution in sub-cellular regions, it was not possible to estimate the relative analyte abundance in different local regions within cells. In this work, we demonstrate as a proof of principle, that analysis of spectral shifts and spectrally integrated emission intensities obtained from emission spectral profiles of the colorimetric sensor (for mercury ions) can indeed provide information on relative proportion of analyte in local regions within individual cells. The methodology relies on construction of two dimensional (2D) scatter plots of integrated intensity and spectral shifts from various regions within individual cells, from which semi-quantitative information on sensor concentration and the relative analyte present with respect to local sensor concentrations can be obtained. We show that correlation between spectral shifts with their respective integrated intensities in various local regions within/between cell(s) can provide information on relative proportion of analyte therein. Although this method is still semi-qualitative due to few limitations, the use of more than one spectral parameter to extract information on relative abundance of analyte widens the scope and opens up future possibilities of quantitative analyte detection *in vivo*, especially when sensors are non-uniformly distributed within cells (or amongst different cells in an ensemble).

[3] For a FRET based sensor, identical intensity ratio (obtained for two energetic regions) for two microscopic locations in a cell imply very similar ratio of analyte-bound sensors and free (unbound) sensors. If local concentration of sensors is higher for one of the locations, the relative proportion of analyte must also be higher therein. Similarly, two spatial locations with diverse intensity ratios may not necessarily imply that analyte concentrations are very different, as this would also depend on the amount of sensory probes present within the two local regions.

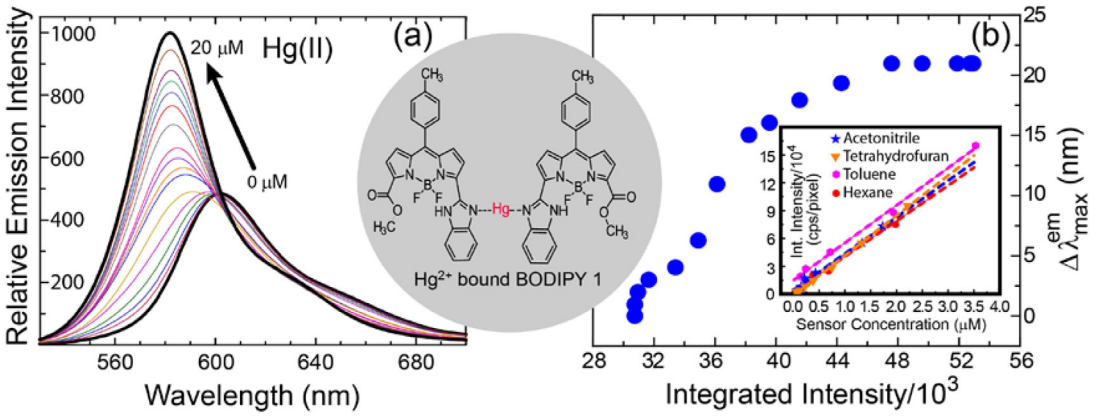

Figure 1. (a) Fluorescence emission spectra of BODIPY **1** (1 μM) upon titration with Hg(II) ($Hg(ClO_4)_2$) in CH_3CN/PBS (7:3; v/v, pH 7.4) solution. (b) Correlation between integrated intensity and magnitude of spectral shift ($\Delta\lambda^{em}_{max} = 604 - \lambda^{em}_{max}$) at different equivalents of mercury, depicting binding with Hg (II) increases both parameters in a systematic manner. Inset of (b) depicts how the emission intensity of BODIPY **1** change with sensor concentration in solvents of different polarity, as obtained by spectrally resolved fluorescence imaging in our microscope setup. The chemical structure of BODIPY **1** Hg(II) adduct is partially overlaid on top of (a) and (b). Figure 1(a) has been adapted with permission from [17] Copyright (2013) American Chemical Society.

2. Results and discussion

2.1. Colorometric and fluorescence sensing in solution

Spectrophotometric titration measurements in solution (figure 1) revealed that emission spectra of BODIPY **1** undergoes a continuous blue-shift in conjunction with an increase in the relative intensity upon Hg(II) binding. We found that while the intensity of emission almost doubles at high Hg(II) concentrations, the emission maxima (λ^{em}_{max}) change from 604 to 582 nm. Similarly, the absorption band of BODIPY **1** centered at 577 nm also undergoes a continuous blue-shift (figure S1(a), supporting information (stacks.iop.org/MAF/5/014003/mmedia)) through an isosbestic point at ~545 nm, which suggests inter-conversion of two species attributed to free sensors and the mercury ion bound sensors, respectively [17]. A correlation diagram (figure 1(b)) of shift in transition energy and emission intensities of BODIPY **1** at different analyte concentration reveal that λ^{em}_{max} its is more sensitive for the detection of Hg(II) at relatively lower concentrations, where emission intensity changes are nominal. In contrast, the shift in λ^{em}_{max} of BODIPY **1** saturates earlier at higher analyte concentrations as compared to the emission intensity (figures 1(b) and S1(b), supporting information). While this will be important in context of analyte detection in cellular media (*vide infra*), it is clear from figure 1(b) (and figure S1(b)) that both these spectral parameters can be used to obtain the sensing efficiency of BODIPY **1**. We also note that the emission intensity of BODIPY **1** changes linearly (upto ~4 μM) without much being affected (<20%) by solvent polarity (figure 1(b), inset), and can therefore be used as a parameter to scale the sensor concentrations in media of different polarity.

2.2. Fluorescence intensity analyses in cellular media

To test the ability of fluorescence intensity enhancement based sensing capability of BODIPY **1** in cellular environments, scanning confocal microscopy (SCM) was performed on BODIPY **1** labelled cells in the absence and presence of different amounts of Hg (II) (0, 10 and 30 μM incubation for 10 min), the results of which are shown in figures 2(a)–(c). These SCM images show that sensor labelling of cells is not uniform; some cells are brighter as compared to others (figures 2(a)–(c)). A closer inspection of magnified SCM images (shown as inset) revealed that the intensity not only varies significantly from cell to cell (marked as 1 and 2 in figure 2(a)), but also within the individual cells. It is therefore not surprising that some cells in absence of Hg(II) are brighter than cells in presence of Hg(II) (compare 2 of 2a and 3 of 2b). Further we noticed, that the cytoplasm and cell membranes are preferentially labelled and the extent of BODIPY **1** penetration into the nuclei is considerably less as compared to rest of the cell (inset figures 2(a)–(c)). Moreover, irrespective of the analyte (Hg(II)) concentration, highly localized ($\leqslant 1$ μm^2) emissive regions are found to be present in the cytoplasm within each cell, which are likely to be hydrophobic cellular organelles such as vacuoles and lipid droplets (vesicles) where the sensor dye tends to accumulate [31] (for convenience, these localized bright emission spots will be referred to as 'vesicles'). Nonetheless, these measurements show that the fluorescence intensity of labelled cells, on an average, increase by ~2 fold in presence of analyte (figure 2), consistent with the solution studies of Hg(II) binding of BODIPY **1** (figures 1(a), (b) and S1(b)) [17].

To understand how emission intensities of local microscopic regions within individual cells vary in presence of Hg (II), fluorescence intensity distribution

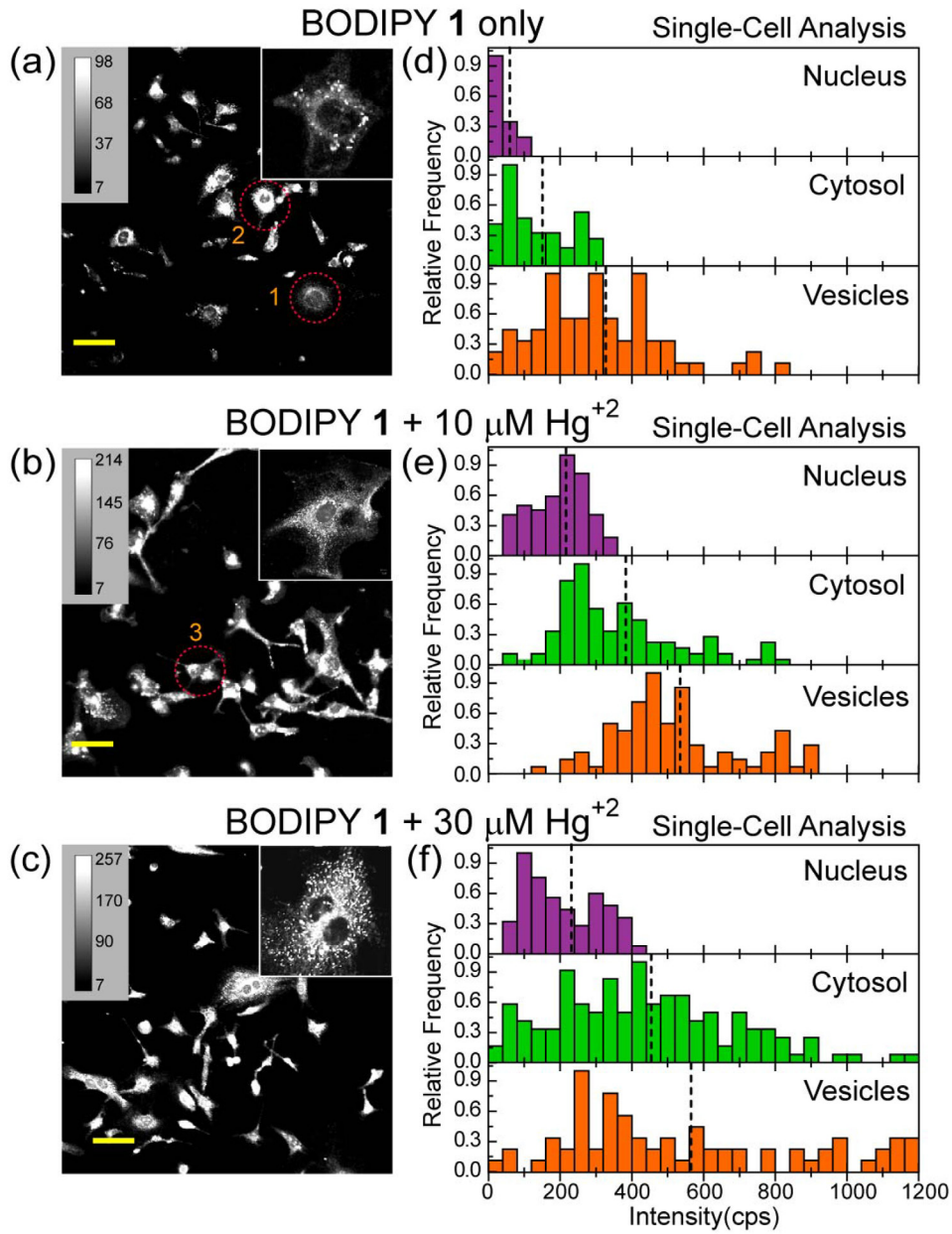

Figure 2. SCM images of BODIPY **1** (1 μM) labelled MDA-MB-231 cells in the absence (a) and presence of 10 μM (b) and 30 μM (c) of Hg(II) (incubation concentrations). The cells marked with open circles are discussed in the text for labelling inhomogeneity between cells (1 and 2) within a sample, and high intensity in absence of Hg(II) as compared to when Hg(II) is present (2 and 3). The magnified images of single cells are shown as the inset to clearly visualize the labelling heterogeneity within the cell. The scale bar is the same for all the images, 50 μm. Intensity distributions from distinguishable cellular features (nucleus, cytosol and vesicles) for 0 μM (d) 10 μM (e) and 30 μM (f) Hg(II). These distributions are constructed for the average counts of 0.05 μm^2 area from the TIRF images provided in figure S2. The vertical dashed line in each plot of (d)–(f) shows the mean value of emission intensity.

analyses was performed at higher magnification (60×) using a wide field total internal reflection (TIRF) microscope where single-frame snapshots were collected to minimize dye (sensor) photobleaching. TIRF images of individual cells obtained in the absence and presence of two incubation concentrations of Hg (II) are shown in figures S2(a)–(c), from which it is clear that the distribution of BODIPY **1** is extremely inhomogeneous within each cell. The intensity distributions obtained from various sub-microscopic regions (~0.05 μm^2) within the nucleus, cytoplasm and vesicles within a single cell are shown in figures 2(d)–(f). We find that the average intensity within the nucleus in absence (figure 2(d)) and presence of Hg(II) (figures 2(e) and (f)) is considerably less as compared to that in the cytoplasm, arising from lesser penetration of the sensors in the nucleus. Further, while the average intensities (dashed vertical lines in figure 2) progressively increase with increasing analyte concentration in various cellular regions (cytosol, nucleus etc), the intensity distribution within the cytoplasm (as well as for vesicles therein) is extremely wide, especially in the presence of the analyte. In fact, the spatial intensity distributions of BODIPY **1** within the nucleus, cyto-

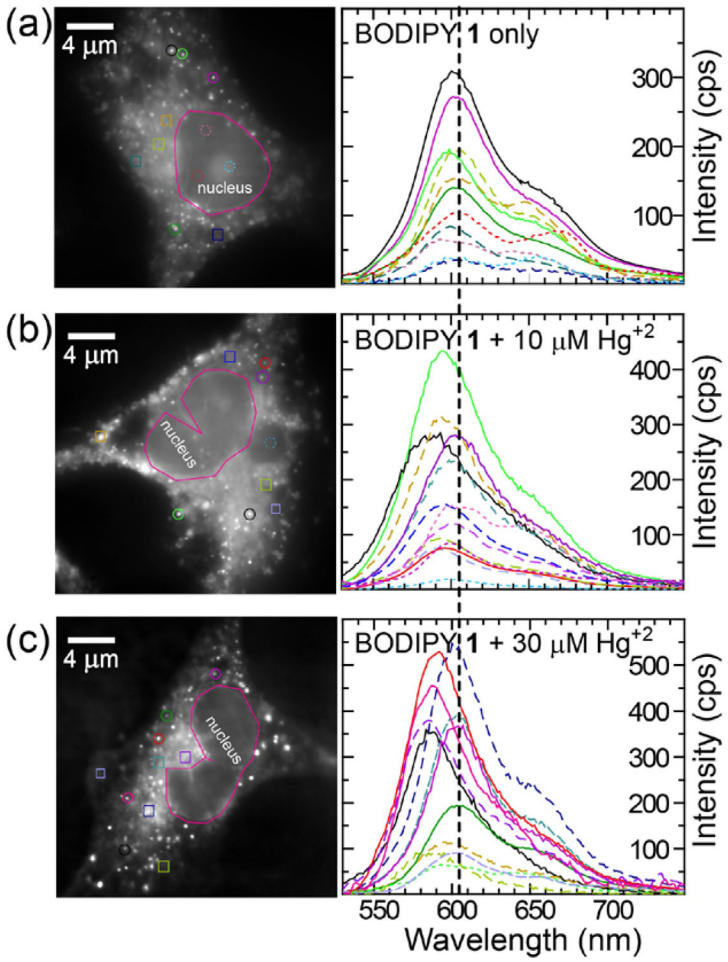

Figure 3. A data set of wide field TIRF images on individual cells in the absence (a) and presence of 10 μM (b) and 30 μM (c) of Hg(II). In each image local regions within the cells are marked using circles and squares for which fluorescence emission spectra is shown in the right of each image. The emission spectra collected from nucleus (dotted lines), cytoplasm (dashed lines) and vesicles (solid lines) are color matched with various regions in corresponding left panel intensity images. The vertical dotted line at 604 nm represents the mean value of λ_{max}^{em} for >100 individual emission spectra in absence of Hg(II).

plasm as well as vesicles overlap considerably in the absence and presence of mercury, which exemplifies that intensity enhancement of BODIPY **1** within a local (sub-cellular) region can arise either from binding to analyte or due to heterogeneity of sensor distribution in localized regions within each cell. This demonstrates that the emission intensity of the sensor cannot serve as a reliable parameter for relative comparison of *analyte* concentrations in different local regions within a single cell, or even between two different cells in the sub-ensemble. However, as BODIPY **1** is also a colorimetric sensor which undergoes a continuous blue shift in the emission envelope upon binding to increasing amounts of mercury, spatially resolved fluorescence spectroscopy measurements can provide additional information on the analyte sensing efficacy within local micro regions of individual cells.

2.3. Spatially resolved spectral analysis within cells using SRFM

Spatially-resolved emission spectra of BODIPY**1** collected over various regions within individual cells in the absence and presence of Hg(II) are shown in figure 3, along with TIRF intensity images of the cells from which the spectral profiles were acquired. Here, representative emission spectra from various sub-microscopic regions (~0.25 μm^2, color matched) of the nucleus (dotted lines), cytoplasm (dashed lines) and vesicles (solid lines) are shown. For a comparison of intensity and transition energies of different cells within the ensemble, spatially-resolved emission spectra from another set of cells from the same samples (at each analyte concentration) are shown in figure S2. In absence of analyte, the emission spectra of BODIPY **1** in cells (figures 3(a) and S2(a)) typically shows a maximum (λ_{max}^{em}) at ~604 $\pm$ 2 nm with a secondary peak (shoulder) between 650 and 670 nm, similar to that observed in solution (figure 1(a)). In contrast, with increasing incubation concentrations of mercury, the λ_{max}^{em} (figures 3(b), (c) and S2(b), (c)) shows blue-shift to different extents at various local regions of the cell, and as a result, the mean value of λ_{max}^{em} ($\langle\lambda_{max}\rangle$) shifts to lower wavelengths (*vide infra*). While there is lack of any obvious correlation between the spectral peak positions and emission intensity for different local regions within a cell under a fixed Hg(II) concentration, on an average,

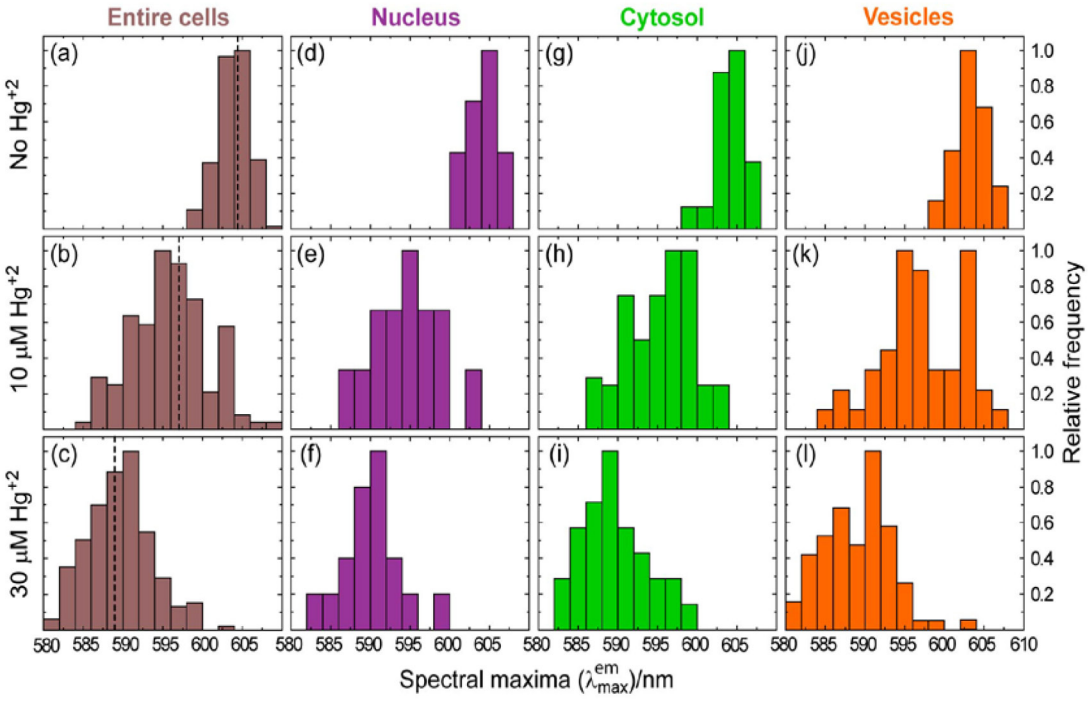

Figure 4. Distributions of λ^{em}_{max} positions for entire cell ((a)–(c)) nucleus ((d)–(f)), cytoplasm ((g)–(i)) and vesicles ((j)–(l)) in the absence ((a), (d), (g), (j)) and presence of 10 μM ((b), (e), (h), (k)) and 30 μM ((c), (f), (i), (l)) Hg(II). The distributions are made from data points from 5 sets of single cells (>100 data points) for each mercury concentration.

the emission intensity is augmented with increasing analyte, consistent with solution data (figure 1).

Due to non-uniformity in the transition energy in presence of analyte, it is challenging to extract any meaningful information on analyte sensing using few emission spectral profiles. Therefore, the λ^{em}_{max} were evaluated for ~100 emission spectra over various local regions of the entire cell (for 5 sets of cells), the frequency distribution for which are shown in figures 4(a)–(c) in absence and presence of analyte. Further, to understand and compare the behaviours of the sensing efficiency in different regions of the cell, the distributions of λ^{em}_{max} ($P(\lambda^{em}_{max})$) obtained from the nucleus (d)–(f), cytoplasm (g)–(i) and vesicles (j)–(l) have been constructed separately. It is apparent that for each region within cells (as well as for the entire cell), the $P(\lambda^{em}_{max})$ shifts to lower wavelengths with increasing concentration of the analyte; for 10 μM and 30 μM Hg(II), the $\langle\lambda_{max}\rangle$ changes to ~597 nm and ~589 nm, respectively. In contrast to the relatively wide $P(\lambda^{em}_{max})$ shown in figures 4(b) (c) and (e), (f), (h), (i), (k), (l), we find that distributions are quite narrow in absence of Hg(II) (figures 4(a), (d), (g) and (j)). This suggests that spectral blue-shifts of BODIPY **1** observed in the presence of mercury ions are unlikely to arise from varying polarity of the local environments within sub-cellular environments, but rather from analyte detection [17].

It is important to note however, neither do the systematic shifts in $P(\lambda^{em}_{max})$ with increasing incubation concentrations of mercury imply larger amounts of analyte being present in the cells, nor does the wide distribution indicate the non-uniformity of relative proportion of mercury in various microenvironments within each cell. This is simply because the extent of spectral shift (λ^{em}_{max}) depends on the *relative proportion of analyte with respect to the sensor*, and not on the *absolute* amounts of analyte present in any given microscopic domain. In other words, the extent of observed spectral shift will essentially be the same as long as the ratio of the sensor and the analyte (or the ratio of free sensor to analyte bound sensor) in different local region remains unchanged. Since the spatial distribution of the sensor is extremely non-uniform over different microscopic regions of cells (figures 2 and 3), comparison of spectral shift will not provide any meaningful information on the relative proportions of the analyte in different local regions. Therefore, a single-parameter observable, such as the spectral shift in this case, is not sufficient to estimate the relative concentrations of analyte within any two microscopic sub-cellular regions. Interestingly, for BODIPY **1**, the fluorescence intensity increases linearly for the range of sensor concentration used in incubation media (figure 1(b), inset). Moreover, effect of polarity on fluorescence intensity of BODIPY **1** is also within 20% for the wide range of sensor concentrations. Thus, it is reasonable to infer that the measured fluorescence intensities can also provide semi-quantitative estimates of the relative concentration of the sensor probe molecules within cellular environments.

As mentioned earlier, the advantage of acquiring spatially-resolved emission spectra is that both peak position as well as the integrated emission intensity can be extracted simultaneously for any local region within cells. While the location of spectral maxima (and hence the extent of blue-shift) portrays the relative proportion of sensor with respect to the analyte in any given local

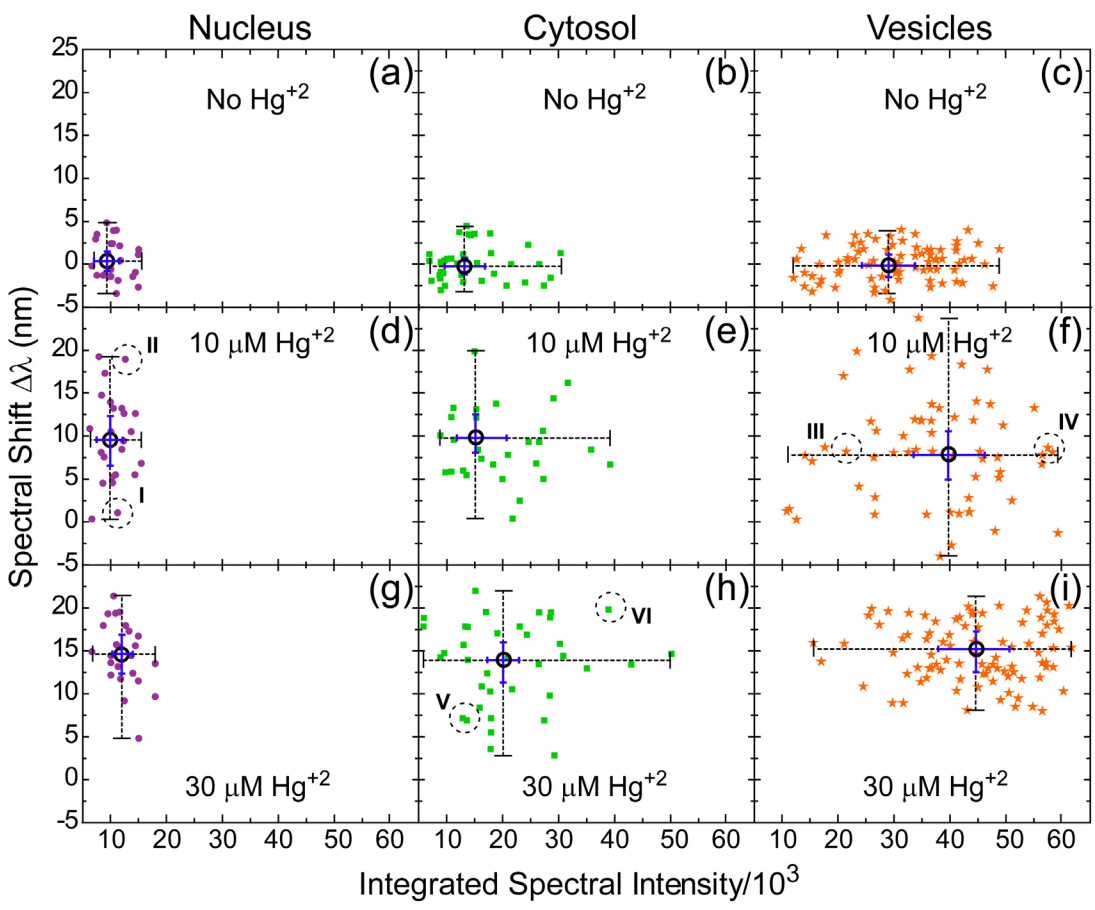

Figure 5. Plot of magnitude of spectral shift ($\Delta\lambda^{em}_{max}$=604 − λ^{em}_{max}) against integrated emission intensity for nucleus (circle), cytoplasm (square) and vesicles (stars) in the absence (a)–(c) and the presence of 10 μM (d)–(f) and 30 μM (g)–(i) Hg (II) for five sets of cells. The spread of $\Delta\lambda$ and intensity is indicated using dotted and solid lines, lengths of which represent their respective range and standard deviation, while the average values of measured parameters are the intersection of two perpendicular lines (indicated with bold circles). Different regions (marked I–VI) compared in the text are highlighted with dotted circles.

region, the integrated emission intensity can be used to estimate the local sensor concentrations (within a factor of ~2 error). Therefore, it is possible to compare any two microscopic regions within a single cell (or even amongst different cells) to extract information on the sensor concentration as well as relative sensor to analyte ratios if the extent of spectral shifts ($\Delta\lambda^{em}_{max}$) are plotted against the integrated intensities for each spectra. For example, it can be inferred that for any two local regions within the cell which have similar intensity, the region for which the observed $\Delta\lambda^{em}_{max}$ is large must have a higher abundance of the analyte. To verify this hypothesis, we have extracted the integrated intensities (I_{Int}) and extent of spectral shifts ($\Delta\lambda^{em}_{max}$) from the spatially-resolved spectral data in the absence and presence of different amounts of Hg(II). Figure 5 shows scatter plots of the spectral shift against integrated intensities from various local regions within nucleus, cytoplasm as well as the vesicles.

In absence of mercury (figures 5(a)–(c)), it is observed that $\Delta\lambda^{em}_{max}$ has almost equal spread ($\sigma^0{}_{\Delta\lambda^{em}_{max}} = 2.5$ nm) for nucleus, cytoplasm and vesicles. However the average intensity ($\langle I_{Int}\rangle$) and its spread (σ_{Int}) increase from nucleus to cytoplasm to vesicles, reflecting the increased amount of sensor present in these locations. Moreover, the spread of intensity (σ_{Int}) is large for cytoplasm and vesicles, which implies that sensor distribution therein is much more non-uniform as compared to that in the nucleus. In presence of different amounts of the analyte (figures 5(d)–(i)), $\langle I_{Int}\rangle$ in the various subcellular regions increases slightly due to mercury binding, but this change is not that prominent within the nucleus due to less penetration of sensor molecules therein. The mean $\Delta\lambda^{em}_{max}$ ($\langle\Delta\lambda^{em}_{max}\rangle$) shifts from 9 nm (10 μM) to 14 nm (30 μM) reflecting the increasing amount of mercury within the cells. It is noticed that at higher concentrations (30 μM) of mercury, $\sigma_{\Delta\lambda_{max}}$ decreased more effectively for nucleus (5.5–4.4 nm, figure 5(g)) and vesicles (5.9–5.0 nm, figure 5(i)) as compared to cytoplasm (4.8–4.9 nm, figure 5(h)). This indicates that at higher incubation concentrations, analyte levels within nucleus and vesicles tend to saturate, possibly due to rapid diffusion of mercury (as compared to sensor) in nucleus and cellular reaction against the toxic ions via their encapsulation within vacuoles [31].

In addition, the scatter plot in figure 5 portrays that there is no clear correlation between $\Delta\lambda^{em}_{max}$ and I_{Int} inside cellular environments, which is a conse-

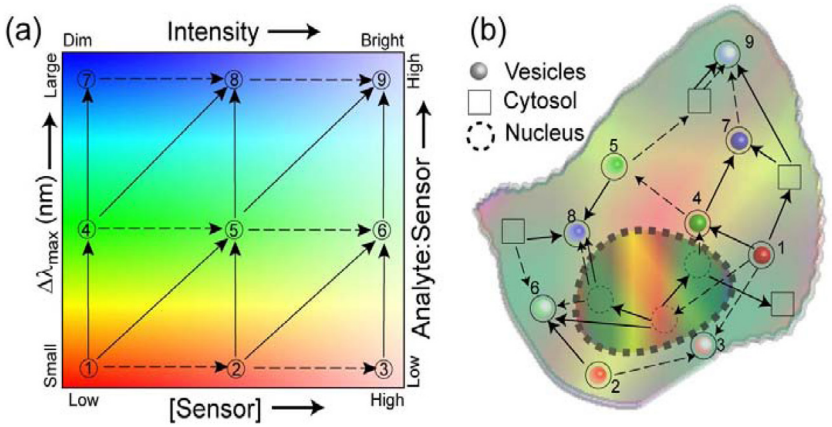

Figure 6. (a) Cartoon showing Intensity versus $\Delta\lambda^{em}_{max}$ plot in relation to the change in sensor and analyte concentration respectively. While the change in $\Delta\lambda^{em}_{max}$ is color coded from red for small to blue for relatively large values, the intensity change is reflected with brightness of each hue. The solid and the dashed arrows indicate the direction in which amount of analyte increase either due to increase in analyte to sensor ratio (solid vertical arrows) or due to increase in total amount of analyte as well as sensor (dashed arrows) or both (solid arrows with positive slope). (b) Various regions within a cell is marked according to figure 6(a) to illustrate how distribution of analyte can potentially be obtained at single cell level using the proposed method.

quence of the non-uniform spatial distribution of sensor. Nonetheless, it is possible to qualitatively estimate the relative distribution of analyte as well as sensor using $\Delta\lambda^{em}_{max}$ versus intensity plots. As a first approximation, we presume that the emission intensity of the sensor remains more or less unaffected due to detection of analyte. This allowed us compare any two data points in the scatter plot acquired from various local regions within the cells for which there is either a significant difference in intensity or spectral shift, or both (marked with dotted circles and numbered **I** through **VI** in figure 5). For a semi-quantitative analysis of analyte distributions within cells to account for effects of local polarity on the intensity and spectral shifts, we have deliberately chosen data sets which are well-separated (by more than 25% and 6 nm, respectively) from within the nucleus, cytoplasm as well as vesicles (figures 5(d)–(i)).

First, consider two locations within cells, such as regions denoted by the **I** and **II** in figure 5(d), with very similar intensity (~11 000 and 12 000 cps) but diverse spectral shifts ($\Delta\lambda^{em}_{max}$ ~ 1 and ~19 nm). Here, intensities indicate that the sensor concentration is likely to be comparable in these two spatial locations, and therefore, the larger spectral shift ($\Delta\lambda^{em}_{max}$) observed for region **II** can only be justified if the local abundance of Hg(II) is significantly more as compared to region **I**. Alternatively, consider two other subcellular regions, such as those marked **III** and **IV** in figure 5(f), where $\Delta\lambda^{em}_{max}$ are very similar (~7.5 nm) while intensities differ considerably (20 000 and 60 000 cps). Here, spectral shifts imply that the relative proportion of analyte with respect to sensor is very similar in both locations. However, as amount of sensor is much more in one region (as indicated by much higher intensity), the abundance of the *analyte* in region **IV** is bound to be significantly more as compared to region **III**. Using a similar argument, it is also possible to perform a relative comparison of two regions for which both $\Delta\lambda^{em}_{max}$ and the emission intensity are high, such as those marked **V** and **VI** in figure 5(h). Here, the relative proportion of analyte to the sensor as well as the concentration of the sensor is more for region **VI** as compared to region **V**. Therefore, it can be inferred that the abundance of *analyte* within region **VI** is considerably higher relative to region **V**.

This method of estimating relative proportion of the analyte, by examining a scatter plot of spectral shift against intensity, can be performed for any two local regions within individual cells as long as the difference between the spectral shifts acquired from the two locations are dissimilar (i.e. higher than $2\sigma^0_{\Delta\lambda_{max}}$, 5 nm). In contrast, similar values of both spectral shifts as well as emission intensity would imply comparable abundance of analyte for two local regions within cells, as well as between different cells in the ensemble. The philosophy of the proposed method of extracting relative distribution of analyte within intracellular environments using SRFM is schematically illustrated in figure 6, where the extent of spectral shift $\Delta\lambda^{em}_{max}$ is depicted as a color (ranging from blue to red, arbitrarily assigned) while the enhancement of intensity is portrayed by the brightness of each color. In this schematic diagram, the vertical arrows reflect the increase in analyte for a fixed sensor concentration (figure 6(a)). On the contrary, the horizontal and the diagonal arrows with a positive slope points to increasing abundance of the sensor as well as the analyte. The cartoon of the cell (figure 6(b)), with different colors as well as brightness depicts the highly inhomogeneous concentration of both the sensor as well as analyte. One can envision collecting spatially-resolved emission spectra over an entire cell, as marked in figure 6(b) (squares and circles), from which both spectral shifts and emission intensities of any two local regions can be extracted to evaluate (or compare) the relative abundance of analyte therein. Such comparison

of emission color and brightness of a spot can be done not only between any two regions of individual cells, but also within the nucleus or cytoplasm, as well as between any two locations amongst two different cells without performing measurements on each cell in absence and presence of the analyte.

While the proposed method is a demonstration of a concept which can allow for relative analyte distributions within subcellular regions using colorimetric sensors, there is enough room for improvement to make this technique more quantitative. There are quite a few reasons which restrict this proposed strategy to be semi-quantitative. First, for the chosen sensory probe (BODIPY **1**), our assumption that '*the binding of sensor to analyte does not seriously affect the intensity*' is not quite accurate, as emission intensity almost doubles under saturation conditions of analyte binding (figure S1(b)), which will be a source of error for estimation of the local (relative) sensor concentrations. It is therefore imperative to develop and use colorimetric fluorogenic sensors with relatively large changes in transition energy yet nominal change in emission quantum yield upon analyte binding. Further, there is no quantitative way to perform titration experiments in cellular environments, since increase in analyte (or sensor) concentration in incubation media does not necessarily mean that concentration in the cellular environment will increase proportionately. Potentially, this problem can be alleviated if a separate absorbing unit with distinct absorption spectra is covalently attached with the sensor to obtain information on sensor's concentration (independently) within a local subcellular region via spatially resolved absorption spectroscopy [32]. Finally, there is also a need to develop new sensory probes which have nominal solvatochromic effect to make the proposed technique more quantitative.

3. Conclusions

A dual-parameter sensing method using spatially-resolved fluorescence spectroscopy is proposed to obtain semi-quantitative information on spatial distribution of analyte within heterogeneous media such as individual cells as well as amongst different cells in the ensemble. To demonstrate the proof of principle, we use BODIPY sensor for mercury ions which undergo emission spectral blue-shift upon analyte binding both in solution and in cellular media. This method of analyses using SRFM can potentially be useful for fluorogenic sensors which show subtle spectral changes due to analyte detection, difficult to resolve using bandpass filters.

Our results indicate that single-parameter measurements, such as intracellular (localized) emission intensities of a colorimetric sensor, are not reliable for estimation of relative analyte concentration due to spatially non-uniform labelling of sensors within cellular media. In contrast, the collection of emission spectral profiles of sensors from various local domains within subcellular regions (such as nuclei, cytosol and lipid vesicles) can concurrently yield information on two spectral parameters, namely, the integrated fluorescence intensity and the transition energy. We show that 2D scatter plots of these spectral parameters can be used to obtain correlation between integrated emission intensity (which qualitatively reflects local density of sensors) and the extent of spectral shift due to sensing (which is related to relative amount of analyte with respect to sensor) within a local subcellular region. We demonstrate, using three different concentration regimes of incubated analyte, how such scatter plots can be analysed to compare any two local subcellular regions, and thereby extract information of the spatial distribution of analyte within single cells. Although several issues need to be addressed for quantitative analyte estimation, the proposed method using SRFM can prove to be a useful alternate tool to monitor spatiotemporal distribution of analyte in heterogeneous cellular media.

3.1. Materials and methods

The synthesis of BODIPY sensor and its characterization is published elsewhere [17]. All other chemicals used for cell culture and fixation were purchased from HiMedia Laboratories, Mumbai, India. MDA-MB-231 human breast adenocarcinoma cells were obtained from the National Centre for Cell Science, Pune, India. These cells were further cultured in complete medium comprised of Dulbecco's Modified Eagle's Medium (DMEM, catalogue no. AL007A) supplemented with 10% fetal bovine serum (FBS; Catalogue No RM1112) and 1% antibiotics (penicillin-streptomycin; catalogue No A001A) at 37 °C under 5% CO_2 atmosphere. The cultured cells were treated with trypsin-EDTA (catalogue No TCL007) for trypsonization and seeded on to glass bottomed Petri dishes at the density of 5000 cells per square cm and incubated overnight [17].

For fluorescence imaging of living cells using, 1 μl of BODIPY **1** (1 mM) was added to the medium of the cells (1 ml) and incubated for 20 min. Thereafter, DMEM was removed from the Petri dish, cells were washed twice with PBS (without calcium and magnesium, catalogue No TL1006, pH = 7.4) and fresh DMEM was added. For imaging fixed cells in absence and presence of Hg(II), MDA-MB-231 cells were incubated with 0 μl (without Hg), 10 μl and 30 μl of 1 mM Hg(II) in 1 ml of DMEM for 10 min. Just before they rounded up (within ~15 min), the cells were fixed with 4% paraformaldehyde for 15–20 min. This was followed by incubation of all the three samples (Hg^{2+} 0, 10 and 30 μl) with BODIPY **1** (1 μl of 1 mM) for 20 min. Then the cells were washed with PBS twice, and the fresh medium was added before performing optical microscopic measurement.

3.1.1. *Confocal microscopy*

The cells were visualized under a scanning confocal microscope (Carl Zeiss LSM 510) capable of taking

fluorescence images using excitation wavelength of 543 nm and an emission band-pass (BP) filter (560–615 nm). The same samples were used for high resolution fluorescence imaging and spatially resolved spectroscopic measurements.

3.1.2. Spatially resolved fluorescence spectroscopy

A home-built through-the-objective total internal reflection fluorescence (TIRF) microscopy setup based on an inverted optical microscope (Nikon TE2000U) was used to perform spectrally resolved fluorescence microscopy of various regions within the cell(s). A 532 nm DPSS laser (30 mW) was used to excite the sample via 60×, 1.49 NA, oil objective (Nikon, Apo TIRF). Typically, ~1 mW excitation powers were used to illuminate ~30 × 30 μm^2 area of the sample. The fluorescence emission was collected through the same objective and imaged using cooled interline CCD camera (DVC 1412AM) through appropriate dichroic mirror and emission filters (Semrock). Spatially resolved fluorescence image and emission spectra from different local regions (0.25 μm^2) of fixed cells were obtained simultaneously using a combination of an adjustable slit and a transmission grating (300 l mm^{-1}) placed in front of the CCD. Obtained spectral images were background flattened and analysed using freely available ImageJ (NIH) and Origin 7.5. The emission profiles from spectrally resolved images were obtained by integrating 3 pixels along vertical (spatial) direction. Wavelength calibration was done using several laser lines and emission spectra were corrected for CCD efficiency resulting in spectral resolution of ~4 nm. The spectral parameters such as peak positions and integrated intensity for each local region were obtained by fitting raw data with Gaussian function. All spectrally resolved images were obtained at ~100 W cm^{-2} excitation powers and 500 ms exposure time. All the measurements were carried out at 295 K under ambient conditions.

Acknowledgments

DKS, SD and SM acknowledge the Council of Scientific and Industrial Research (CSIR), India and IIT Bombay for PhD fellowships. AC acknowledges IRCC IIT Bombay and CSIR, India for initial funding and a research grant Scheme: 80(0070)/08/EMR-II. DKS acknowledges IRCC IIT Bombay for research associateship. MI thanks IIT Bombay for an institute postdoctoral fellowship and the 'Start-Up Research Grant' no. SB/FT/CS 098/2013 from SERB Department of Science and Technology (Govt. of India).

Notes

The authors declare no competing financial interest.

References

[1] Johnson I 1998 Fluorescent probes for living cells *Histochem. J.* **30** 123–40
[2] Terai T and Nagano T 2008 Fluorescent probes for bioimaging applications *Curr. Opin. Chem. Biol.* **12** 515–21
[3] Carter K P, Young A M and Palmer A E 2014 Fluorescent sensors for measuring metal ions in living systems *Chem. Rev.* **114** 4564–601
[4] Domaille D W, Zeng L and Chang C J 2010 Visualizing ascorbate-triggered release of labile copper within living cells using a ratiometric fluorescent sensor *J. Am. Chem. Soc.* **132** 1194–5
[5] Ueno T and Nagano T 2011 Fluorescent probes for sensing and imaging *Nat. Methods* **8** 642–5
[6] Basabe-Desmonts L, Reinhoudt D N and Crego-Calama M 2007 Design of fluorescent materials for chemical sensing *Chem. Soc. Rev.* **36** 993–1017
[7] Qian X, Xiao Y, Xu Y, Guo X, Qian J and Zhu W 2010 'Alive' dyes as fluorescent sensors: fluorophore, mechanism, receptor and images in living cells *Chem. Commun.* **46** 6418–36
[8] Gunnlaugsson T, Glynn M, Tocci (nee Hussey) G M, Kruger P E and Pfeffer F M 2006 Anion recognition and sensing in organic and aqueous media using luminescent and colorimetric sensors *Coord. Chem. Rev.* **250** 3094–117
[9] Abebe F A, Eribal C S, Ramakrishna G and Sinn E 2011 A 'turn-on' fluorescent sensor for the selective detection of cobalt and nickel ions in aqueous media *Tetrahedron Lett.* **52** 5554–8
[10] Chen L, Yang L, Li H, Gao Y, Deng D, Wu Y and Ma L 2011 Tridentate lysine-based fluorescent sensor for Hg(II) in aqueous solution *Inorg. Chem.* **50** 10028–32
[11] Zeng L, Miller E W, Pralle A, Isacoff E Y and Chang C J 2006 A selective turn-on fluorescent sensor for imaging copper in living cells *J. Am. Chem. Soc.* **128** 10–1
[12] Qian Y, Karpus J, Kabil O, Zhang S-Y, Zhu H-L, Banerjee R, Zhao J and He C 2011 Selective fluorescent probes for live-cell monitoring of sulphide *Nat. Commun.* **2** 495
[13] Wang P, Wu J, Su P, Shan C, Zhou P, Ge Y, Liu D, Liu W and Tang Y 2016 A novel fluorescent chemosensor based on tetra-peptides for detecting zinc ions in aqueous solutions and live *Cells. J. Mater. Chem.* B **4** 4526
[14] Domaille D W, Que E L and Chang C J 2008 Synthetic fluorescent sensors for studying the cell biology of metals *Nat. Chem. Biol.* **4** 168–75
[15] Szmacinski H and Lakowicz J R 1995 Fluorescence lifetime-based sensing and imaging *Sensors Actuators* **29** 16–24
[16] Qian F, Zhang C, Zhang Y, He W, Gao X, Hu P and Guo Z 2009 Visible light excitable Zn^{2+} fluorescent sensor derived from an intramolecular charge transfer fluorophore and its *in vitro* and *in vivo* application *J. Am. Chem. Soc.* **131** 1460–8
[17] Madhu S, Sharma D K, Basu S K, Jadhav S, Chowdhury A and Ravikanth M 2013 Sensing Hg(II) *in vitro* and *in vivo* using a benzimidazole substituted BODIPY *Inorg. Chem.* **52** 11136–45
[18] Agarwalla H, Gangopadhyay M, Sharma D K, Basu S K, Jadhav S, Chowdhury A and Das A 2015 Fluorescent probes for the detection of cyanide ions in aqueous medium: cellular uptake and assay for β-glucosidase and hydroxynitrile lyase *J. Mater. Chem.* B **3** 9148–56
[19] Paredes J M, Giron M D, Ruedas-rama M J, Orte A, Crovetto L, Talavera E M, Salto R and Alvarez-pez J M 2013 Real-time phosphate sensing in living cells using fluorescence lifetime imaging microscopy (FLIM) *J. Phys. Chem.* B **117** 8143–9
[20] Hötzer B, Ivanov R, Brumbarova T, Bauer P and Jung G 2012 Visualization of Cu^{2+} uptake and release in plant cells by fluorescence lifetime imaging microscopy *FEBS J.* **279** 410–9
[21] Berezin M Y and Achilefu S 2010 Fluorescence lifetime measurements and biological imaging *Chem. Rev.* **110** 2641–84
[22] Suhling K *et al* 2015 Fluorescence lifetime imaging (FLIM): basic concepts and some recent developments *Med. Photon.* **27** 3–40

[23] Peng X et al 2011 Fluorescence ratiometry and fluorescence lifetime imaging: using a single molecular sensor for dual mode imaging of cellular viscosity *J. Am. Chem. Soc.* **133** 6626–35
[24] Okabe K, Inada N, Gota C, Harada Y, Funatsu T and Uchiyama S 2012 Intracellular temperature mapping with a fluorescent polymeric thermometer and fluorescence lifetime imaging microscopy *Nat. Commun.* **3** 705
[25] Madhu S, Basu S K, Jadhav S and Ravikanth M 2013 3,5-Diformyl-borondipyrromethene for selective detection of cyanide anion *Analyst* **138** 299–306
[26] Dean K M, Qin Y and Palmer A E 2012 Visualizing metal ions in cells: an overview of analytical techniques, approaches, and probes *Biochim. Biophys. Acta* **1823** 1406–15
[27] Kim H N, Ren W X, Kim J S and Yoon J 2012 Fluorescent and colorimetric sensors for detection of lead, cadmium, and mercury ions *Chem. Soc. Rev.* **41** 3210–44
[28] Hu B, Hu L L, Chen M L and Wang J H 2013 A FRET ratiometric fluorescence sensing system for mercury detection and intracellular colorimetric imaging in live Hela cells *Biosens. Bioelectron.* **49** 499–505
[29] Marín M J, Galindo F, Thomas P and Russell D A 2012 Localized intracellular pH measurement using a ratiometric photoinduced electron-transfer-based nanosensor *Angew. Chem. Int. Ed. Engl.* **51** 9657–61
[30] Kuimova M K 2012 Mapping viscosity in cells using molecular rotors *Phys. Chem. Chem. Phys.* **14** 12671–86
[31] Nies D H 1999 Microbial heavy-metal resistance *Appl. Microbiol. Biotechnol.* **51** 730–50
[32] Sharma D K and Chowdhury A 2013 Spectrally resolved optical microscopy using a transmission grating spectrograph: importance of spatial selection *Analyst* **139** 473–81